

Phase diagram for the extended Hubbard model on a square lattice

Sebastião dos Anjos Sousa-Júnior,¹ Natanael C. Costa,¹ and Raimundo R. dos Santos¹

¹*Instituto de Física, Universidade Federal do Rio de Janeiro Cx.P. 68.528, 21941-972 Rio de Janeiro RJ, Brazil*

The Extended Hubbard model describes electron-electron interactions and is commonly used to understand various phenomena in strongly correlated systems. In this paper, we focus on investigating the phase diagram of this model, which considers a nearest neighbor interaction, V , in addition to the on-site term U . To perform our study, we utilize the determinant quantum Monte Carlo method simulations, where the average sign of the determinant is used to extract information about the quantum critical points. When both U and V are positive, the on-site term favors antiferromagnetism (AFM), while the extended interaction favors the formation of a charge density wave (CDW). In cases where at least one of the interactions is negative, superconductivity competes with the above-mentioned phases, and the system displays phase separation for intense attractive extended interaction. Our findings indicate that only s -wave and d -wave pairing symmetries exist in such scenarios.

Soon after the discovery of high-temperature cuprate superconductors [1–3], a widespread consensus was formed around the idea that the basic physical mechanism leading to superconductivity was contained in the two-dimensional Hubbard model: pairing would emerge from strong antiferromagnetic (AFM) fluctuations arising from the competition between itinerancy (hopping) and localisation, the latter driven by an on-site repulsion of strength U [4, 5]. Despite its simplicity, the repulsive Hubbard model has eluded an unambiguous characterisation of superconductivity. Subsequently, it was proposed [6] that antiferromagnetic fluctuations could actually lead to an additional effective nearest-neighbour attractive interaction, V . The ground state phase diagram for the extended Hubbard model (EHM) in one dimension and at half filling has been known for some time; see, e.g. Ref. [7]. For different values and signs of U and V , one finds phases such as charge-density wave (CDW), spin-density wave (SDW), and s -wave superconductivity. A phase separated (PS) state appears for sufficiently large $-V$, e.g., half of the lattice with doubly occupied sites, and the other half empty, in the strong $-V$ regime. Less conventional phases such as bond-ordered wave [7] and p -wave superconducting [8] have also been proposed to fit into the diagram.

In two dimensions, while one expects the ground state phase diagram at half filling to share similarities with that for the one-dimensional model, the picture is far from settled. Indeed, different methods agree with the existence of a CDW-AFM transition near $U = 4V$ [9–12]. Nonetheless, the square lattice topology in principle allows for a wider range of pairing symmetries to be stabilised in the $V < 0$ region, which has proved very hard to probe theoretically. Weak-coupling methods [10, 13] may not fully capture the competition between the tendencies of phase separating and forming pairs of different symmetries, such as s and $d_{x^2-y^2}$. Numerically exact diagonalisation of the Hamiltonian is currently restricted to 4×4 systems, so that the prediction of a p -wave paired state [14] may not stand for larger systems. Quantum Monte Carlo (QMC) simulations [15, 16], on

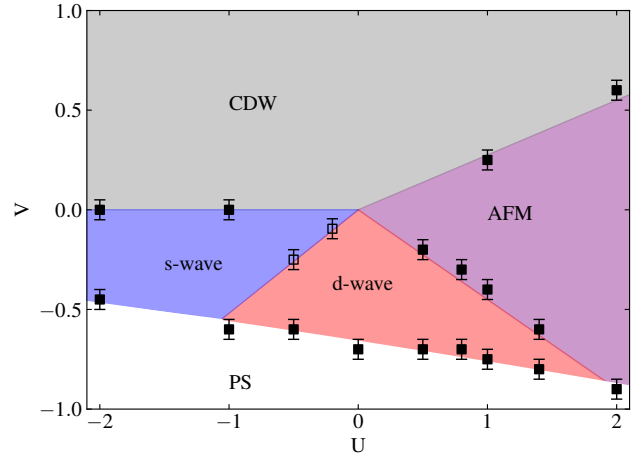


FIG. 1. Ground state phase diagram for the extended Hubbard model at half filling, obtained through our DQMC simulations; U and V are on-site and NN couplings, respectively. Filled symbols are estimates for critical points obtained through the joint analyses of structure factors and $\langle s \rangle$; the latter played no part in determining the critical points represented by empty symbols. CDW stands for charge density wave, AFM for antiferromagnetic, s -wave and d -wave are superconducting phases, and PS denotes phase separation. Lines through data points are guides to the eye.

the other hand, suffer from the infamous ‘minus-sign problem’ [16–20]: when the effective Boltzmann factor (given by a product of fermionic determinants) becomes negative, averages are taken with it in absolute value, at the expense of dividing by its own average, $\langle s \rangle$, thus introducing excessive noise when $\langle s \rangle \ll 1$. Recent studies of the EHM through QMC simulations were restricted to parameter regimes where the minus-sign problem was not too severe, so that the focus was mostly on the CDW-AFM transition [21]. The inescapable conclusion is that so far the overall knowledge of the EHM phase diagram is, at best, semi-qualitative.

In light of the recent suggestion [22, 23] that a severely degraded $\langle s \rangle$ may actually be used to pinpoint

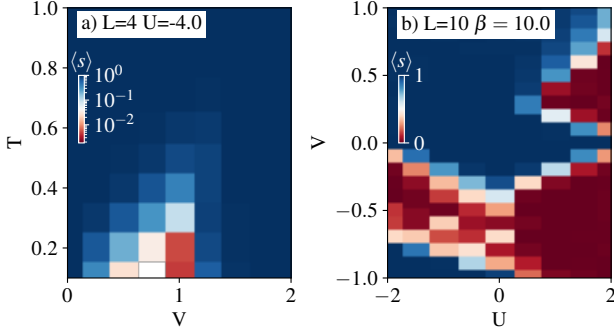


FIG. 2. a) Contour plot of the average sign for $U = 4$ on a 4×4 lattice at half filling. b) Contour plot of the average sign for $T = 0.1$ in the V - U plane for a 10×10 lattice.

phase transition points and boundaries, a thorough investigation of the EHM through determinant QMC (DQMC) simulations is certainly in order. With this in mind, here we report on the results for the ground state phase diagram at half-filling in the whole V - U parameter space with an unprecedented accuracy; our main findings are highlighted in Fig. 1.

The Hamiltonian for the EHM reads,

$$\mathcal{H} = -t \sum_{\langle \mathbf{i}, \mathbf{j} \rangle} (c_{\mathbf{i}\sigma}^\dagger c_{\mathbf{j}\sigma} + \text{H.c.}) - \mu \sum_{\mathbf{i}, \sigma} n_{\mathbf{i}, \sigma} + U \sum_{\mathbf{i}} n_{\mathbf{i}\uparrow} n_{\mathbf{i}\downarrow} + V \sum_{\langle \mathbf{i}, \mathbf{j} \rangle} n_{\mathbf{i}} n_{\mathbf{j}}, \quad (1)$$

where \mathbf{i} and \mathbf{j} denote sites of a square lattice, with $\langle \mathbf{i}, \mathbf{j} \rangle$ restricting the sums to nearest neighbour (NN) sites. In standard second-quantised notation, the first term describes fermionic hopping (energy scale t), the second controls the band filling through the chemical potential, μ , while the third and fourth terms describe the on-site and NN interactions, with strengths U and V , respectively. Hereafter, the chemical potential is set to $\mu = U/2 + 4V$ to yield a half-filled band (by virtue of particle-hole symmetry), and energies is expressed in units of t .

In the DQMC method [16–20], discrete Hubbard-Stratonovich (HS) transformations [24] are used to express the quartic interactions in quadratic forms. This leads to 5 auxiliary fields on any given site \mathbf{i} : 1 from the on-site term, and 4 from the bonds emanating from it [9]; see, e.g., the Supplemental Materials. The non-commutation between the one-body and the two-body terms of the Hamiltonian is taken care of through a Suzuki-Trotter decomposition, which adds an imaginary-time dimension, $L_\tau = \beta/\Delta\tau$, with β being the inverse temperature, and $\Delta\tau$ the discrete time step. The trace over the fermionic degrees of freedom can then be performed, leading to the product of determinants alluded to before, which weigh the configurations of the HS Ising fields sampled by importance, as in usual Monte Carlo methods [16–20].

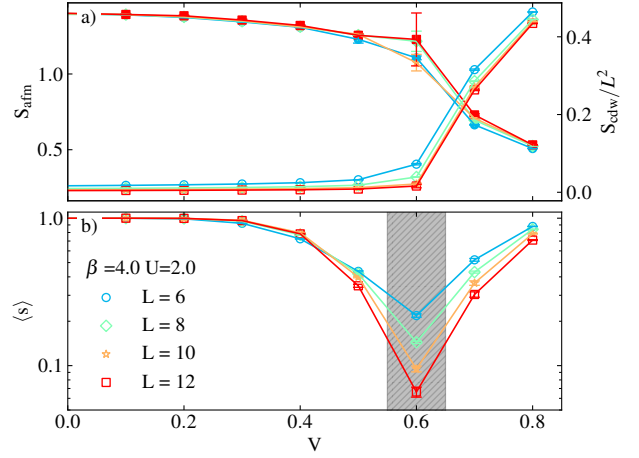


FIG. 3. (a) Spin structure factor (filled symbols, left vertical scale) and scaled charge structure factor (empty symbols, right vertical scale), and (b) average sign as functions of V . All data are for fixed $U = 2$ and $\beta = 4$, and different linear system sizes, L . The grey bar highlights the region where $\langle s \rangle$ dips.

The type of ordering is characterised by quantities such as the (staggered) charge structure factor,

$$S_{\text{cdw}} = \frac{1}{N} \sum_{\mathbf{i}, \mathbf{j}} (-1)^{|\mathbf{i}-\mathbf{j}|} \langle (n_{\mathbf{i}, \uparrow} + n_{\mathbf{i}, \downarrow})(n_{\mathbf{j}, \uparrow} + n_{\mathbf{j}, \downarrow}) \rangle, \quad (2)$$

the antiferromagnetic structure factor,

$$S_{\text{afm}} = \frac{1}{N} \sum_{\mathbf{i}, \mathbf{j}} (-1)^{|\mathbf{i}-\mathbf{j}|} \langle S_{\mathbf{i}}^z S_{\mathbf{j}}^z \rangle, \quad (3)$$

and the pairing structure factor,

$$P_{\text{sc}}(\alpha) = \frac{1}{N} \sum_{\mathbf{i}, \mathbf{j}} \langle \Delta_\alpha(\mathbf{i}) \Delta_\alpha^\dagger(\mathbf{j}) \rangle, \quad (4)$$

with

$$\Delta_\alpha(\mathbf{i}) = \sum_{\mathbf{a}} f_\alpha(\mathbf{a}) c_{\mathbf{i}\downarrow} c_{\mathbf{i}+\mathbf{a}\uparrow}. \quad (5)$$

In the above equations, $N = L \times L$ is the number of sites for a linear size L , $(-1)^{|\mathbf{i}-\mathbf{j}|}$ is ± 1 if \mathbf{i} and \mathbf{j} are on the same or opposite sublattices, $S_{\mathbf{i}}^z = (n_{\mathbf{i}\uparrow} - n_{\mathbf{i}\downarrow})$ is the z -component of the spin operator, and $f_\alpha(\mathbf{a})$ is the form factor for a given pair-wave symmetry, $\alpha = s, d, p$ [25]. In some circumstances, it is more appropriate to calculate the pair susceptibility

$$\chi_{\text{sc}}^\alpha(\beta) = \frac{1}{N} \sum_{\mathbf{i}, \mathbf{j}} \int_0^\beta d\tau \langle \Delta_{\mathbf{i}, \alpha}(\tau) \Delta_{\mathbf{j}, \alpha}^\dagger(0) \rangle, \quad (6)$$

with $\Delta_\alpha(\mathbf{i}, \tau) = \sum_{\mathbf{a}} f_\alpha(\mathbf{a}) c_{\mathbf{i}\downarrow}(\tau) c_{\mathbf{i}+\mathbf{a}\uparrow}(\tau)$, and $c_{\mathbf{i}\sigma}(\tau) = e^{\tau \mathcal{H}} c_{\mathbf{i}\sigma} e^{-\tau \mathcal{H}}$, which provides a stronger signal of pairing properties. As mentioned before, $\langle s \rangle$, which is

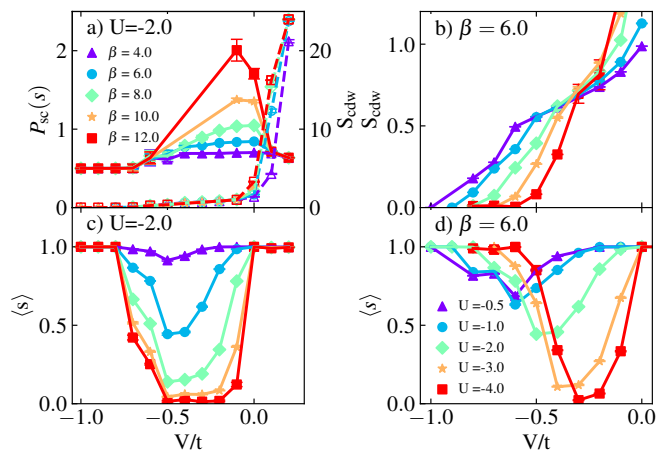


FIG. 4. (a) s -pairing structure factor (full lines, left vertical axis) and charge structure factor (dashed line, right vertical axis), and (c) average sign as functions of V at fixed U , for different temperatures; (b) charge structure factor [notice the different scale from (a)] and (d) average sign as functions of V , at fixed inverse temperature, for different values of the on-site attraction.

automatically calculated in the simulations, will also play a crucial role in our analyses.

When $V \neq 0$ one cannot guarantee that $\langle s \rangle = 1$ even at half filling. As shown in Fig. 2 (a), the average sign decreases as the temperature is lowered, and it is seen to be particularly worse near $V = 1$. Recalling that the phase boundary for the SDW-CDW transition is $V_c \approx U/4$, the minimum of $\langle s \rangle$ at $V = 1$ can hardly be regarded as fortuitous. A mapping of $\langle s \rangle$ in the V - U plane at a fixed low temperature is shown in Fig. 2 (b). Apart from the second quadrant ($U < 0, V > 0$), one sees that there are regions where $\langle s \rangle \ll 1$, surrounded by less severe ones. In what follows we combine analyses of $\langle s \rangle$ with the quantities defined by Eqs. (2)-(4) to obtain the phase boundaries in Fig. 1.

We start with the transition between the AFM (Mott) phase and the CDW phase. As indicated in Fig. 3 (a), increasing V causes a sharp decrease of S_{afm} and a sharp increase of S_{cdw} thus indicating a phase transition at $V_c = 0.6 \pm 0.05$, where the error reflects the V increments in Fig. 3 (a). This is accompanied by a dip in $\langle s \rangle$ at the same value of V ; see Fig. 3 (b). The behaviour for $U = 1$ is similar, leading to $V_c = 0.2 \pm 0.05$, so that, similarly to the 1D case [26], the AFM-CDW critical line lies slightly above the strong-coupling prediction, $V_c = U/4$.

Let us now focus on the second ($U < 0, V > 0$) and third ($U < 0, V < 0$) quadrants of the parameter space. Figure 4 (a) shows that the charge structure factor decreases steadily as one crosses the $V = 0$ line towards $V < 0$, at fixed $U = -2$; by contrast, the s -wave pairing structure factor increases steadily with increasing β on the $V < 0$ side. This behaviour is consistent with the fact that exactly at $V = 0$ one reaches the attractive Hubbard model, which definitely displays a CDW state coexisting

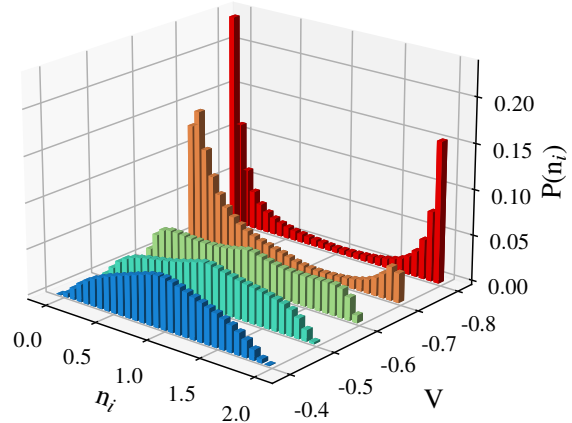


FIG. 5. Density probability distribution for several values of V with $U = -0.5$ and $\beta = 6.0$. As the intensity of the attractive interaction increases the shape of the histograms undergoes from a single peaked to a double peaked distribution.

with an s -wave superconducting state [27, 28]: one deals effectively with a three-component order parameter, one for CDW and two for the superconductivity. Further decrease in V causes a suppression of s -wave pairing correlations, as one enters the PS region, at $V = -0.45 \pm 0.05$ for $U = -2$. Interestingly, Figure 4 (c) shows that as the temperature decreases, the dip in $\langle s \rangle$ deepens and widens throughout the superconducting phase; in the PS region, $\langle s \rangle$ returns to 1. Thus the sharp drops in $\langle s \rangle$ indicate the boundaries of the superconducting phase with the CDW and PS regions. Figure 4 (b) provides an interesting insight into the behaviour of the charge structure factor, by keeping the temperature fixed at $\beta = 6$, and examining how the plots evolve with U . Two regimes can be distinguished: one in which charge correlations are enhanced as $|U|$ increases, and another in which they decrease as $|U|$ increases. The analysis of Fig. 4 (a) hence suggests that this change indicates the entrance into the PS region. This is again in accordance with the behaviour of $\langle s \rangle$ at fixed β and for different values of U , depicted in Fig. 4 (d): the dip occurs at smaller values of V as U increases. These findings are summarised in Fig. 1.

The transition to the PS state deserves a complementary look, by examining the density distribution shown in Fig. 5, generated by collecting the values of n_i over the DQMC runs. For $V = 0$, the distributions are represented by singly peaked histograms (not shown), centred at $n = 1$. As V decreases, the distributions first broaden, still with a peak at $n = 1$, but a change to doubly-peaked at $n = 0$ and $n = 2$ takes place, interpreted as a signature of a phase separated state. In Fig. 5, this occurs at $V \approx -0.6$, which also marks the dip in $\langle s \rangle$ for $U = -0.5$; see Fig. 4 (d).

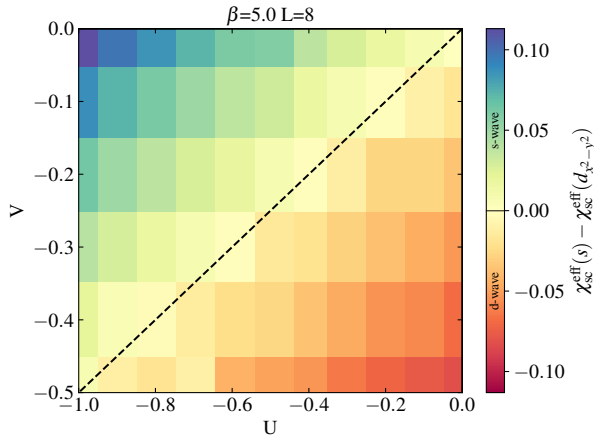


FIG. 6. a) Contour plot of the difference between s -wave and d -wave effective pairing susceptibilities for $\beta = 5.0$ and $L = 8$.

Returning to the SC state, we must settle the issue of pairing symmetries. To this end, we start with the difference between the effective pairing susceptibilities with s and $d_{x^2-y^2}$ symmetries, which presumably dominate the third quadrant. At this point, we investigate the effective pair (vertex) susceptibility, i.e., $\chi_{sc}^{\text{eff}}(\alpha) = \chi_{sc}(\alpha) - \bar{\chi}_{sc}(\alpha)$, with $\bar{\chi}_{\alpha(sc)}$ being the noninteracting susceptibility [25]. A positive (negative) response of $\chi_{sc}^{\text{eff}}(\alpha)$ signals an enhancement (weakening) of pair correlations for the corresponding α -wave symmetry. From Fig. 6 we see that the region above the line $V = U/2$ is dominated by s -wave pairing, while the region below the line is dominated by $d_{x^2-y^2}$ -wave pairing. Interestingly, $\langle s \rangle$ shows no dip at this transition; we may attribute this to the lack of change in the number of components of the order parameter on either side of the transition.

Moving on to the fourth quadrant, $V < 0$ and $U > 0$, Fig. 7(a) follows how the spin structure factor changes as V is increased. Below $V \approx -0.7$, S_{afm} is quite insensitive to the temperature. For $-0.7 \lesssim V \lesssim -0.25$, S_{afm} actually decreases as the temperature increases, while the superconducting structure factors are enhanced in this interval [see Fig. 7(b) and (d)], with $P_{sc}(d_{x^2-y^2})$ tending to dominate over $P_{sc}(p_x)$. The dip in $\langle s \rangle$ at $V \approx -0.7$ provides additional support to the interpretation of a PS- d -wave transition at this point in the diagram. Beyond $V \approx -0.25$, S_{afm} increases as the temperature is lowered, which is also accompanied by a dip in $\langle s \rangle$: this signals a d -wave-AFM transition. By repeating these analyses for other values of $U > 0$, we obtain the critical curve in Fig. 1, in which the error stems from the resolution of the crossings in Fig. 7(a).

In view of the recent suggestion that a p -wave SC state could be stabilised, we examined pairing structure factors and susceptibilities. Typical data are shown in Fig. 8: while for $L = 4$, d -wave and p -wave structure factors are degenerate, and dominate over s -wave, for

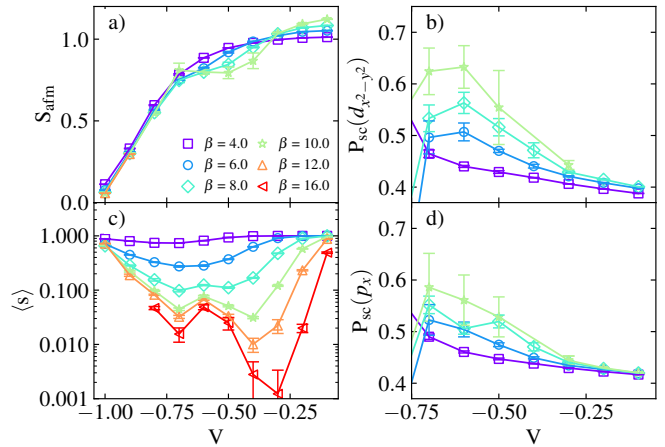


FIG. 7. a) Spin structure factor, b) d -wave pairing correlation function c) Average sign and d) p -wave pairing correlation function as a function of V for $U = 0.8$ with $L = 6$.

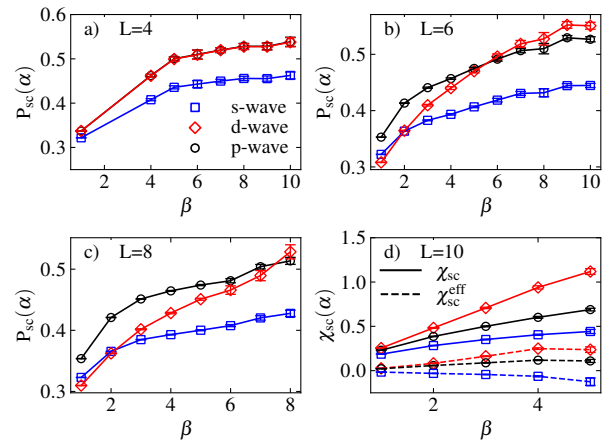


FIG. 8. (a)-(c) Pairing structure factors and (d) pairing susceptibilities as functions of the inverse temperature for different symmetries, for the sizes shown. All data are for $U = 0.5$, and $V = -0.5$.

larger systems d -wave pairing become dominant as $\beta \rightarrow \infty$. This tendency is confirmed by the behaviour of the pairing susceptibilities (both bare and effective), for $L = 10$; see Fig. 8(d) As discussed in Ref. 10, d -wave pairing should dominate in the $V < 0$ region, due to the nesting of the Fermi surface, while the p -wave would be favoured in absence of this feature. Interestingly, this is somehow observed in our results of Fig. 8: the smaller the system size is, the weaker nesting effects are, leading to a spurious p -wave enhancement.

In summary, we have resolved long standing issues relative to the ground state phase diagram of the half-filled extended Hubbard model on a square lattice, such as the pairing symmetries of the superconducting phase, and locations of phase boundaries in all four quadrants of the $U - V$ plane. Indeed, through

our DQMC simulations, accurate boundaries involving antiferromagnetic, charge-density wave, s -wave and d -wave superconducting, and phase-separated phases were determined. The presence of a d -wave superconducting phase over a reasonably wide region in the parameter space adds credence to the use of the EHM as a minimal single-band model to describe the high- T_c cuprates [6]. Also worth noticing is that the ‘minus-sign’ problem of QMC simulations was overcome by performing extensive simulations, and by using the recently proposed connection between critical points and strong dips in $\langle s \rangle$. Indeed, the multitude of phases in the diagram allowed us to verify that dips in $\langle s \rangle$ only occur at transitions involving different universality classes, such as AFM-CDW, AFM-SC, SC-PS, and CDW-SC, but not

between s - and d -waves.

ACKNOWLEDGMENTS

The authors are grateful to the Brazilian Agencies Conselho Nacional de Desenvolvimento Científico e Tecnológico (CNPq), Coordenação de Aperfeiçoamento de Pessoal de Ensino Superior (CAPES), and Instituto Nacional de Ciência e Tecnologia de Informação Quântica (INCT-IQ) for funding this project. N.C.C. acknowledges support from FAPERJ Grant No. E-26/200.258/2023 - SEI-260003/000623/2023, and CNPq Grant No. 313065/2021-7.

-
- [1] J. G. Bednorz and K. A. Müller, “Possible high- T_c superconductivity in the Ba-La-Cu-O system,” *Zeitschrift für Physik B Condensed Matter* **64**, 189–193 (1986).
- [2] Chandra M. Varma, “Colloquium: Linear in temperature resistivity and associated mysteries including high temperature superconductivity,” *Rev. Mod. Phys.* **92**, 031001 (2020).
- [3] Xingjiang Zhou, Wei-Sheng Lee, Masatoshi Imada, Nandini Trivedi, Philip Phillips, Hae-Young Kee, Päivi Törmä, and Mikhail Erements, “High-temperature superconductivity,” *Nature Reviews Physics* **3**, 462–465 (2021).
- [4] P. W. Anderson, “The resonating valence bond state in La_2CuO_4 and superconductivity,” *Science* **235**, 1196–1198 (1987).
- [5] V. J. Emery, “Theory of high- T_c superconductivity in oxides,” *Phys. Rev. Lett.* **58**, 2794–2797 (1987).
- [6] D. J. Scalapino, “A common thread: The pairing interaction for unconventional superconductors,” *Rev. Mod. Phys.* **84**, 1383–1417 (2012).
- [7] H. Q. Lin, E. R. Gagliano, D. K. Campbell, E. H. Fradkin, and J. E. Gubernatis, “The phase diagram of the one-dimensional extended Hubbard model,” in *The Hubbard Model: Its Physics and Mathematical Physics*, edited by Dionys Baeriswyl, David K. Campbell, Jose M. P. Carmelo, Francisco Guinea, and Enrique Louis (Springer US, Boston, MA, 1995) pp. 315–326.
- [8] Bo Xiao, Javier Robledo Moreno, Matthew Fishman, Dries Sels, Ehsan Khatami, and Richard Scalettar, “Extracting Off-Diagonal Order from Diagonal Basis Measurements,” (2022), [arXiv:2209.10565](https://arxiv.org/abs/2209.10565) [cond-mat.str-el].
- [9] Y. Zhang and J. Callaway, “Extended Hubbard model in two dimensions,” *Phys. Rev. B* **39**, 9397–9404 (1989).
- [10] Wen-Min Huang, Chen-Yen Lai, Chuntai Shi, and Shan-Wen Tsai, “Unconventional superconducting phases for the two-dimensional extended Hubbard model on a square lattice,” *Phys. Rev. B* **88**, 054504 (2013).
- [11] M. Vandelli, V. Harkov, E. A. Stepanov, J. Gukelberger, E. Kozik, A. Rubio, and A. I. Lichtenstein, “Dual boson diagrammatic Monte Carlo approach applied to the extended Hubbard model,” *Phys. Rev. B* **102**, 195109 (2020).
- [12] Meng Yao, Da Wang, and Qiang-Hua Wang, “Determinant quantum Monte Carlo for the half-filled Hubbard model with nonlocal density-density interactions,” *Phys. Rev. B* **106**, 195121 (2022).
- [13] Sebastian Wolf, Thomas L. Schmidt, and Stephan Rachel, “Unconventional superconductivity in the extended Hubbard model: Weak-coupling renormalization group,” *Phys. Rev. B* **98**, 174515 (2018).
- [14] Wei-Chih Chen, Yao Wang, and Cheng-Chien Chen, “Superconducting phases of the square-lattice extended hubbard model,” (2022), [arXiv:2206.01119](https://arxiv.org/abs/2206.01119) [cond-mat.supr-con].
- [15] R. Blankenbecler, D. J. Scalapino, and R. L. Sugar, “Monte Carlo calculations of coupled boson-fermion systems. I,” *Phys. Rev. D* **24**, 2278–2286 (1981).
- [16] J. E. Hirsch, “Two-dimensional Hubbard model: Numerical simulation study,” *Phys. Rev. B* **31**, 4403–4419 (1985).
- [17] R. T. Scalettar, N. E. Bickers, and D. J. Scalapino, “Competition of pairing and Peierls-charge-density-wave correlations in a two-dimensional electron-phonon model,” *Phys. Rev. B* **40**, 197–200 (1989).
- [18] Naoki Kawashima, “Quantum Monte Carlo Methods,” *Progress of Theoretical Physics Supplement* **145**, 138–149 (2002).
- [19] Raimundo R. dos Santos, “Introduction to quantum Monte Carlo simulations for fermionic systems,” *Braz. J. Phys.* **33**, 63–54 (2003).
- [20] Federico Becca and Sandro Sorella, *Quantum Monte Carlo Approaches for Correlated Systems* (Cambridge University Press, 2017).
- [21] Alexander Sushcheyev and Stefan Wessel, “Thermodynamics of the metal-insulator transition in the extended Hubbard model from determinantal quantum Monte Carlo,” *Phys. Rev. B* **106**, 155121 (2022).
- [22] R. Mondaini, S. Tarat, and R. T. Scalettar, “Quantum critical points and the sign problem,” *Science* **375**, 418–424 (2022).
- [23] Rubem Mondaini, Sabyasachi Tarat, and Richard T. Scalettar, “Universality and Critical Exponents of the

- Fermion Sign Problem,” (2022), [arXiv:2207.09026](https://arxiv.org/abs/2207.09026) [cond-mat.str-el].
- [24] J. E. Hirsch, “Discrete Hubbard-Stratonovich transformation for fermion lattice models,” *Phys. Rev. B* **28**, 4059–4061 (1983).
- [25] S. R. White, D. J. Scalapino, R. L. Sugar, N. E. Bickers, and R. T. Scalettar, “Attractive and repulsive pairing interaction vertices for the two-dimensional Hubbard model,” *Phys. Rev. B* **39**, 839–842 (1989).
- [26] J. E. Hirsch, “Charge-Density-Wave to Spin-Density-Wave Transition in the Extended Hubbard Model,” *Phys. Rev. Lett.* **53**, 2327–2330 (1984).
- [27] R. Micnas, J. Ranninger, and S. Robaszkiewicz, “Superconductivity in narrow-band systems with local nonretarded attractive interactions,” *Rev. Mod. Phys.* **62**, 113–171 (1990).
- [28] Rodrigo A. Fontenele, Natanael C. Costa, Raimundo R. dos Santos, and Thereza Paiva, “Two-dimensional attractive Hubbard model and the BCS-BEC crossover,” *Phys. Rev. B* **105**, 184502 (2022).
- [29] Louk Rademaker, Steve Johnston, Jan Zaanen, and Jeroen van den Brink, “Determinant quantum Monte Carlo study of exciton condensation in the bilayer Hubbard model,” *Phys. Rev. B* **88**, 235115 (2013).
- [30] James Gubernatis, Naoki Kawashima, and Philipp Werner, “Determinant method,” in *Quantum Monte Carlo Methods: Algorithms for Lattice Models* (Cambridge University Press, 2016) p. 180–213.

Supplemental Material for: Phase diagram for the extended Hubbard model on a square lattice

The DQMC algorithm: To take into account the interaction terms of (1) one first performs a Suzuki-Trotter decomposition,

$$e^{-\beta\mathcal{H}} \approx (e^{-\Delta\tau\mathcal{H}_k} e^{-\Delta\tau\mathcal{H}_U} e^{-\Delta\tau\mathcal{H}_V})^M + \mathcal{O}(\Delta\tau^2) \quad (\text{S1})$$

where the 2D problem is mapped into a 3D system with the new dimension being the imaginary time axis, and the inverse of the temperature β is cut into M discrete intervals with length $\Delta\tau = \beta/M$. The quartic terms of \mathcal{H}_U and \mathcal{H}_V are expressed in a quadratic form using the Hubbard-Stratonovich transformation [9, 24],

$$e^{-\Delta\tau W n_{i\sigma} n_{j\sigma'}} = \frac{1}{2} \sum_{x_\nu = \pm 1} e^{[\alpha x_\nu (n_{i\sigma} - n_{j\sigma'}) - \frac{\Delta\tau W}{2} (n_{i\sigma} + n_{j\sigma'})]} \quad (\text{S2})$$

with $\cosh \alpha = \exp(\Delta\tau W/2)$, and $W = \{U, V\}$ depending if it is the on-site or the extended Hubbard term. The second term in the argument of the exponential of Eq. (S2) is cancelled by setting the chemical potential $\mu = U/2 + 4V$ at half-filling. One auxiliary field $x_0(\mathbf{i}, l)$ is defined for each lattice site \mathbf{i} and time slice l , for the on-site interaction of \mathcal{H}_U . Since \mathcal{H}_V is expanded as

$$V n_{\mathbf{i}} n_{\mathbf{j}} = V (n_{\mathbf{i}\uparrow} n_{\mathbf{j}\uparrow} + n_{\mathbf{i}\uparrow} n_{\mathbf{j}\downarrow} + n_{\mathbf{i}\downarrow} n_{\mathbf{j}\uparrow} + n_{\mathbf{i}\downarrow} n_{\mathbf{j}\downarrow}), \quad (\text{S3})$$

four auxiliary fields for each bond between nearest neighbors sites \mathbf{i} and \mathbf{j} are defined, namely $x_1(\mathbf{i}, \mathbf{j}, l)$, $x_2(\mathbf{i}, \mathbf{j}, l)$, $x_3(\mathbf{i}, \mathbf{j}, l)$, and $x_4(\mathbf{i}, \mathbf{j}, l)$. Working on a square lattice with periodic boundary conditions with N sites, and consequently $2 \times N$ bonds, results in a total of $8 \times N \times M$ auxiliary fields for the extended term in addition to the $N \times M$ auxiliary fields for the on-site term. The partition function of the system then becomes,

$$\mathcal{Z} = \frac{1}{2^{9NM}} \sum_{x_\nu = \pm 1} \prod_{\sigma} \det A^\sigma(x_0, x_1, x_2, x_3, x_4), \quad (\text{S4})$$

with,

$$A^\sigma(x_0, x_1, x_2, x_3, x_4) = \mathbb{1} + B^\sigma(M) B^\sigma(M-1) \cdots B^\sigma(1) \quad (\text{S5})$$

and

$$B^\sigma(l) = e^{-\Delta\tau \hat{H}_k} e^{-\Delta\tau \hat{H}_U} e^{-\Delta\tau \hat{H}_V}. \quad (\text{S6})$$

The weight $P(x_\nu)$ of each configuration of auxiliary fields is given by

$$P(x_\nu) = |\det [A^\uparrow A^\downarrow]|. \quad (\text{S7})$$

One can also compute Green's functions [29],

$$G_{\mathbf{i}, \mathbf{j}}^\sigma = \frac{1}{2^{9NM}} \sum_{x_\nu = \pm 1} [A^\sigma]_{\mathbf{i}, \mathbf{j}}^{-1} \prod_{\sigma} \det A^\sigma(x_0, x_1, x_2, x_3, x_4), \quad (\text{S8})$$

and calculate the relevant physical quantities. Since the number of Hubbard-Stratonovich fields (HSF) grows as 2^{9NM} , Ising importance sampling Monte Carlo over $\{x_\nu\}$ is used to analyze the Extended Hubbard model properties. Details of the sampling techniques are discussed in the next topic.

Sampling the Hubbard-Stratonovich fields: The Ising sampling of the HSF consists in sweeps over the sites and bonds trying to make the *flip* $x_\nu \rightarrow -x_\nu$ in each imaginary time slice l . From time to time the physical quantities are measured. For instance, a flip of the x_0 field at a single site and time slice is proposed: if the change is accepted, the new Green's function is computed by $O(N^2)$ operations using the Sherman-Morrison update [30], since the evaluation of the Green's function from Eq. (S8) requires $O(N^3)$ operations. The same approach can be used to update the Green's functions by flipping the x_2 and x_3 fields, which couples the terms with $\sigma \neq \sigma'$ in Eq. (S2), and consequently allows us to use Sherman-Morrison update for G^\uparrow and G^\downarrow separately. The challenge is to update the Green's functions by flipping the x_1 and x_4 fields since they change the Green's functions related to different sites for $\sigma = \sigma'$. Following the procedure described in [29] we use the Woodbury matrix identity, which is a generalized Sherman-Morrison update. The steps to implement this update are detailed in this section.

Starting with a known Green's function at a time slice l given the fields $x_{1(4)}$, we propose a flip $x_{1(4)} \rightarrow x'_{1(4)} = -x_{1(4)}$ in a bond between sites \mathbf{i} and \mathbf{j} for a time slice l individually. Under this change the A^σ matrix becomes,

$$A^\sigma \rightarrow \mathbb{1} - B^\sigma(M) \cdots (\mathbb{1} + \Delta^\sigma) B^\sigma(l) \cdots B^\sigma(1) = A'^\sigma. \quad (\text{S9})$$

The label σ corresponds to spin up and down for x_1 and x_4 respectively. The matrix Δ^σ is diagonal and has only two nonzero elements, namely

$$\begin{aligned} \Delta_{i,i}^\sigma &= \exp[-2x_\nu(\mathbf{i}, \mathbf{j}, l)] - 1 \\ \Delta_{j,j}^\sigma &= \exp[2x_\nu(\mathbf{i}, \mathbf{j}, l)] - 1. \end{aligned} \quad (\text{S10})$$

One can decide whether or not to accept a change using the ratio of determinants [30],

$$R^\sigma = \frac{\det [A'^\sigma]}{\det [A^\sigma]} = \det [\mathbb{1} - \Delta^\sigma (\mathbb{1} - G^\sigma)]. \quad (\text{S11})$$

If the flipping is accepted, by using matrix identities it is possible to write a simple expression for the updated $G^{\sigma'}$ after the flip [30],

$$G'^\sigma \rightarrow G^\sigma - G^\sigma \frac{1}{\mathcal{R}} \Delta^\sigma (\mathbb{1} - G^\sigma). \quad (\text{S12})$$

Due to the sparseness of the matrices \mathcal{R} and Δ^σ , Eq. (S12) can be written in terms of matrix elements [29],

$$G'_{r,s}{}^\sigma \rightarrow G_{r,s}{}^\sigma - \sum_{i,j} G_{r,i}{}^\sigma \mathcal{D}_{i,j} (\delta_{j,s} - G_{j,s}{}^\sigma), \quad (\text{S13})$$

where the matrix \mathcal{D} may be cast in a 2×2 form,

$$\mathcal{D} = \frac{\Delta_{i,i}^\sigma \Delta_{j,j}^\sigma}{R^\sigma} \begin{pmatrix} 1 - G_{j,j}^\sigma + \frac{1}{\Delta_{j,j}^\sigma} & G_{i,j}^\sigma \\ G_{j,i}^\sigma & 1 - G_{i,i}^\sigma + \frac{1}{\Delta_{i,i}^\sigma} \end{pmatrix} \quad (\text{S14})$$

with i and j being the indices of the sites related with the flip of $x_\nu(\mathbf{i}, \mathbf{j}, l)$, and,

$$R^\sigma = \det \mathcal{R} = (\Delta_{i,i}^\sigma (1 - G_{i,i}^\sigma) + 1)(\Delta_{j,j}^\sigma (1 - G_{j,j}^\sigma) + 1) - \Delta_{i,i}^\sigma G_{i,j}^\sigma \Delta_{j,j}^\sigma G_{j,i}^\sigma. \quad (\text{S15})$$

In order to decide whether a proposed change is accepted we used a combination of the Metropolis and the heat-

bath algorithm, similar to the one used in Ref. [29],

$$P_T = \begin{cases} \frac{R^\sigma}{1 + \gamma R^\sigma} & \text{if } R^\sigma \leq 1 \\ \frac{R^\sigma}{\gamma + R^\sigma} & \text{if } R^\sigma > 1 \end{cases} \quad (\text{S16})$$

The parameter γ is tuned self-consistently to achieve an acceptance ratio of approximated 50%.

The order of the flipping attempts is also an important detail in the DQMC method. To achieve better results, four different strategies were tested and the one which provided the best outcome is explained below. A sweep is done over all sites \mathbf{i} trying to flip $x_0(\mathbf{i}, l)$ for $l = 0, 1, 2, \dots, M - 1$, after this, a sweep is done over all bonds trying to flip $x_1(\mathbf{i}, \mathbf{j}, l)$ for $l = 0, 1, 2, \dots, M - 1$ and the same is done for x_2, x_3 and x_4 to complete one Monte Carlo step. Trying to flip all five types of auxiliary fields at the same time, while speeds up the sweep, leads to spurious results for our simulation.

Using the Woodbury update we have performed a few tests in order to verify the accuracy of the results, where the main source of data for comparison is from Ref. [9]. All results were obtained on a 4×4 square lattice with periodic boundary conditions. The parameter of the Trotter decomposition was chosen to be $\Delta\tau = 0.05$. A comparison with exact diagonalization was also done.